

Simultaneous Generation of WDM Chirped Microwave Waveforms Using Integrated Spectral Shapers in Silicon Photonics

Parisa Moslemi, *Student Member, IEEE*, Martin Rochette, *Senior Member, IEEE*, and Lawrence R. Chen, *Senior Member, IEEE, Fellow, OSA*

Abstract—We demonstrate simultaneous generation of wavelength-division-multiplexed chirped microwave waveforms using optical spectral shaping followed by wavelength-to-time mapping. We design two types of integrated spectral shapers based on parallel distributed Fabry–Pérot cavities or an arrayed waveguide grating Sagnac interferometer incorporating linearly chirped waveguide Bragg gratings. The generated waveforms have different central RF frequencies and opposite signs of RF chirp.

Index Terms—Chirped microwave waveforms, RF waveform generation, chirped Bragg gratings, silicon photonics.

I. INTRODUCTION

CHIRPED microwave waveforms are widely used in various applications such as communications (for fiber-wireless and radio-over-fiber networking) and instrumentation, including imaging and sensing (e.g., to improve resolution or increase range) [1]. Generating such waveforms in the electronic domain is limited to the sampling rate of digital electronics that restricts the central frequency, RF chirp, and bandwidth. Using photonic approaches can remove this limitation to obtain chirped waveforms at high central frequencies of up to hundreds of GHz with large RF chirps supporting tens of GHz of bandwidth [2, 3]. In addition, photonic approaches improve manufacturability, stability, reliability, and power consumption [4].

There are several techniques to generate microwave waveforms using photonics such as heterodyne beating of a continuous wave signal with a wavelength-swept laser or a pre-chirped optical pulse [5], frequency multiplication [6], direct space-to-time mapping [7], temporal pulse shaping [8], and optical spectral shaping followed by wavelength-to-time mapping (SS-WTM) [9]. In the latter technique, which is very widespread, the amplitude spectrum of a broadband pulse is first shaped with an optical spectral shaper (OSS) before being propagated through a dispersive medium to map the spectral

content to the time domain. The key component in this process is the OSS as the shaped amplitude spectrum determines the profile, and ultimately characteristics, of the generated waveform. To generate a chirped microwave waveform, we need a periodic OSS followed by a non-linear WTM or an aperiodic OSS followed by a linear WTM.

Despite significant developments on increasing the time-bandwidth product (TBWP) of the chirped microwave waveforms [2, 3], all demonstrations to date involve the generation of only a *single* waveform. On the other hand, generating multiple waveforms with different characteristics (e.g., central frequency or sign of RF chirp) simultaneously enhances the flexibility or increases the functionality in many applications such as improving range in imaging applications or allowing for switching between resolutions [10-12]. Recently, we demonstrated the simultaneous generation of multi-channel, wavelength-division-multiplexed (WDM) chirped microwave waveforms using fiber optics [12, 13]. We obtained two chirped microwave waveforms with different central frequencies and different values of RF chirp or switchable signs of RF chirp using OSSs based on a Sagnac interferometer incorporating superimposed linearly chirped fiber Bragg gratings (LCFBGs) [12] or an arrayed waveguide grating Sagnac interferometer (AWGSI) incorporating LCFBGs [13].

In recent years, the development of integrated OSSs for photonic generation of microwave waveforms has attracted much attention over fiber optic techniques due to compactness and potential for fast reconfiguration [4]. Various integrated OSSs (predominantly in silicon photonics) that generate a single chirped microwave waveform have been implemented. For example, Zhang *et al.* reported an OSS based on a Mach-Zehnder interferometer (MZI) incorporating four (or five) cascaded microring resonators with different radii to generate a chirped microwave waveform with four (or five) cycles at a central frequency of 7.5 GHz and an RF chirp of 17.2 GHz/ns [14]. They also demonstrated an OSS based on a MZI incorporating two tunable linearly chirped waveguide Bragg gratings (LCWBGs) in its two arms generating a symmetrical chirped microwave waveform with the central frequency of 0.14 GHz and RF chirps of 2.7 GHz/ns and -6.1 GHz/ns on either side of the central frequency [15, 16]. Wang *et al.* proposed an OSS consisting of eight tunable microrings with different radii to generate a chirped microwave waveform

Received October 9, 2018. Revised October 9, 2018.

This research was supported in part by the Natural Sciences and Engineering Research Council of Canada and the Fonds de recherche du Québec Nature et technologies.

The authors are with the Department of Electrical Engineering, McGill University, 3480 University Street, Montréal, QC, H3A 0E9, Canada (e-mail: parisa.moslemi@mail.mcgill.ca, martin.rochette@mcgill.ca, lawrence.chen@mcgill.ca).

TABLE I
 PARAMETERS AND CHARACTERISTICS OF THE LCWBGs USED IN THE OSSS

	Parameters			Measured characteristics			
	W_1 / W_2 [nm]	δW [nm]	Λ [nm]	Center wavelength [nm]	% R	3 dB BW [nm]	Grating chirp [nm/mm]
LCWBG-A ₁	700 / 720	10	291	1545.0	50	3.4	13.7
LCWBG-A ₂	700 / 720	10	294	1556.0	50	4.1	13.6
LCWBG-B ₁	500 / 510	5	314	1545.2	70	4.5	14.3
LCWBG-B ₂	500 / 510	5	318	1557.2	70	4.7	14.1

comprising eight cycles [17]. Ma *et al.* demonstrated an OSS based on a distributed Fabry–Pérot cavity (DFPC) which consists of two spatially offset LCWBGs to generate a chirped microwave waveform with a central frequency of 20 GHz and an RF chirp of 12 GHz/ns [18]. Finally, Wang *et al.* described an OSS based on an AWGSI incorporating an LCWBG generating a chirped microwave waveform with a central frequency of 29.6 GHz and 23.8 GHz and an RF chirp of 20 GHz/ns [19].

In this paper, we propose two integrated multi-channel OSS designs based either on parallel DFPCs or an AWGSI incorporating multiple LCWBGs to generate simultaneously multi-channel WDM chirped microwave waveforms.

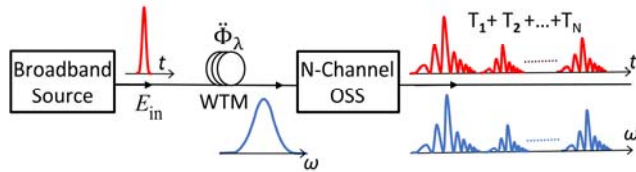


Fig. 1. Schematic of the system generating N different chirped microwave pulses simultaneously based on spectral shaping and WTM technique.

II. DESIGN OF THE MULTI-CHANNEL OPTICAL SPECTRAL SHAPERS

Figure 1 shows the schematic of our approach to generate multi-channel WDM chirped microwave waveforms with different characteristics based on SS-WTM. A broadband source is shaped into WDM spectra using an integrated multi-channel OSS. The shaped spectra are then mapped to the time domain via propagation through a spool of fiber serving as a dispersive medium. Due to the linearity of the system, it does not matter whether OSS is performed before WTM or vice versa. The generated WDM waveforms can then be separated using optical filters.

The proposed multi-channel OSSs are fabricated by electron beam lithography in silicon-on-insulator (SOI). The silicon waveguides have a thickness of 220 nm on top of a 3 μm buried oxide (BOX) layer and have a 2 μm index-matched top oxide cladding (Fig. 2). In both OSSs, LCWBGs are the key components. The LCWBGs are based on sidewall corrugations in strip waveguides. We consider two different designs for the LCWBGs to operate in the C-band, see Fig. 2(a). In one design, denoted LCWBG-A, the waveguide width W_1 varies linearly between 700 nm and 720 nm; the corrugation depth is $\delta W = |W_1 - W_2|/2 = 10$ nm so that correspondingly, W_2 varies

linearly between 720 nm and 740 nm. In the second design, denoted LCWBG-B, the waveguide width varies linearly between $W_1 = 500$ nm and 510 nm and the corrugation depth is $\delta W = 5$ nm (correspondingly, W_2 varies linearly between 510 nm and 520 nm). We use different (constant) grating periods (Λ) to account for the different effective indices of the waveguides (i.e., of different widths) as well as to obtain distinct spectral channels for WDM. Both LCWBGs have 1,000 grating periods. The calculated effective refractive indices (using Lumerical MODE) for strip waveguides with widths of 700 nm and 500 nm are 2.64 and 2.45, respectively. The design parameters of the LCWBGs are given in Table I. Note that tapers are used as necessary to connect the start and end of the LCWBGs to the 500 nm wide strip waveguides that are used for the other components in the OSSs.

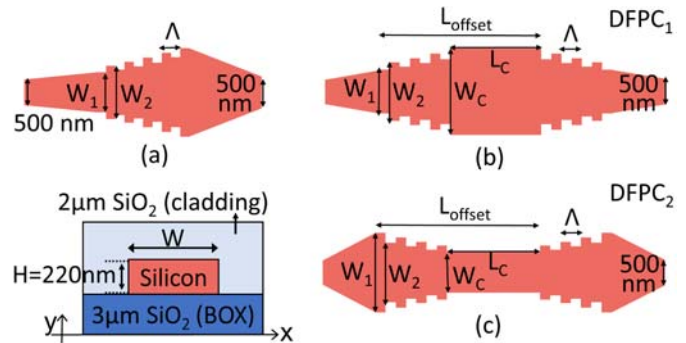


Fig. 2. Schematic of (a) LCWBG based on sidewall corrugations in a strip waveguide (along with waveguide cross-section), (b) and (c) DFPCs that generate opposite signs of RF chirp.

We calculate the grating chirp from $C = 2\Lambda \frac{dn_{eff}}{dz}$, where $\frac{dn_{eff}}{dz}$ is the variation of the effective refractive index (n_{eff}) over the grating length (z). The grating chirps for LCWBG-A and LCWBG-B are 21 nm/mm and 28 nm/mm, respectively. To verify the designs, we fabricated and characterized the spectral responses of the LCWBGs. The measured values for the center wavelength, peak reflectivity, 3 dB bandwidth, and grating chirp (which is estimated from the measured bandwidth and expected grating length) are given in Table I. The measured grating chirps are less than the calculated values due to fabrication errors and errors in obtaining the grating bandwidths due to the spectral response and variations from the vertical grating couplers (VGCs) used for input and output coupling. The VGCs, which are designed for TE operation over the C-

band, have a bandwidth of $\sim 15 - 20$ nm [20]; the measured insertion loss is ~ 7.5 dB/VGC. The VGCs are aligned on the same side of the device and have a pitch of $127 \mu\text{m}$ for coupling with a fiber ribbon array.

A. Multi-channel OSS based on parallel DFPCs

Each DFPC consists of two LCWBGs with opposite grating chirp (i.e., orientation) that are separated spatially by a cavity. Reversing the grating orientations in the DFPC allows for switching the sign of the RF chirp. For example, using a dispersive medium with a dispersion $D > 0$ for WTM, a positive grating orientation, such as the one shown in Fig. 2(b) and denoted DFPC₁, will generate a chirped microwave waveform with a negative RF chirp. On the other hand, for the reverse grating orientation shown in Fig. 2(c) and denoted DFPC₂, the sign of the RF chirp will be positive

The effective cavity length between the two gratings is wavelength dependent and given by [18, 19]:

$$\Delta L_{eff} = \frac{C_1 - C_2}{C_1 C_2} \lambda + L_{offset} + \frac{C_1 - C_2}{C_1 C_2} \lambda_0 \quad (1)$$

where λ_0 is the starting grating wavelength, C_1 and C_2 are the chirps of the LCWBGs, and L_{offset} is the longitudinal offset of the two LCWBGs defined as the cavity length (L_c) plus the LCWBG length [see Figs. 2(b) and 2(c)]. We consider two identical LCWBGs of opposite orientation so that $C_1 = -C_2$.

The grating chirp and the offset length of a DFPC determine the free spectral range (FSR) of the OSS and the corresponding central frequency and RF chirp of the generated waveform. The FSR is given by [22]:

$$FSR = \frac{\lambda_0^2}{2n_{eff}\Delta L_{eff}} \quad (2)$$

After WTM, the instantaneous frequency of the generated waveform becomes:

$$\begin{aligned} f_{RF}(t) &= \frac{2n_{eff}}{\lambda_0^2 D} \Delta L_{eff} \quad (3) \\ &= \frac{2n_{eff}}{\lambda_0^2 D} \left[L_{offset} + \frac{C_1 - C_2}{C_1 C_2} \left(\frac{t}{D} - \lambda_0 \right) \right] \end{aligned}$$

where $\lambda = t/D$ defines the mapping between time and wavelength and D is the dispersion (in [ps/nm]) of the dispersive medium. The central frequency at $t = 0$ is defined by the longitudinal offset L_{offset}

$$f_c = \frac{2n_{eff}}{\lambda_0^2 D} \left[L_{offset} + \frac{C_1 - C_2}{C_1 C_2} (-\lambda_0) \right] \quad (4)$$

and the corresponding RF chirp is

$$\left| \frac{df_{RF}(t)}{dt} \right| = 2n_{eff} \frac{C_1 - C_2}{C_1 C_2} \frac{1}{\lambda_0^2 D^2} \quad (5)$$

Note that for a fixed value of D , the RF chirp is independent of the offset length and depends only on the grating chirp.

The general schematic for a multi-channel OSS based on parallel DFPCs is shown in Fig. 3(a). To demonstrate the principle, we consider simultaneous generation of two chirped microwave waveforms with different central frequencies and opposite signs of RF chirp; we designed two two-channel OSSs incorporating different parallel DFPCs (DFPC₁ and DFPC₂) with different cavity lengths L_c and cavity widths W_c , see Fig.

3(b). The reflected outputs from the two DFPCs are combined via a Y-branch. The first OSS (OSS-1) employs DFPC₁ incorporating LCWBG-A₁ with $L_c = 300 \mu\text{m}$ to generate a waveform at shorter wavelengths, a lower central frequency, and a negative RF chirp, and DFPC₂ incorporating LCWBG-A₂ with $L_c = 600 \mu\text{m}$ to generate a waveform at longer wavelengths, a higher central frequency, and positive RF chirp. The second OSS (OSS-2) employs DFPC₂ incorporating LCWBG-B₁ with $L_c = 600 \mu\text{m}$ to generate a waveform at shorter wavelengths, a higher central frequency, and a positive RF chirp, and DFPC₁ incorporating LCWBG-B₂ with $L_c = 300 \mu\text{m}$ to generate a waveform at longer wavelengths, a lower central frequency, and a negative RF chirp. For OSS-1, the longitudinal offsets for DFPC₁ and DFPC₂ that generate the first and second waveforms are $591 \mu\text{m}$ and $894 \mu\text{m}$, respectively, whereas the corresponding values for OSS-2 are $614 \mu\text{m}$ and $918 \mu\text{m}$. Based on Eqs. (4) and (5), the expected values for the central frequencies and RF chirps of the two generated waveforms for OSS-1 are 23 GHz, 31 GHz and ± 45 GHz/ns, while those of OSS-2 are 30 GHz, 22 GHz and ± 40 GHz/ns respectively.

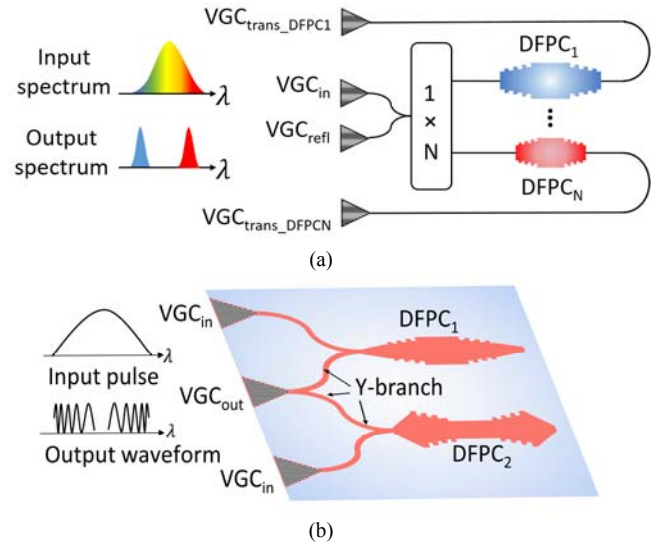


Fig. 3. (a) General schematic of integrated multi-channel OSS based on multiple parallel DFPCs and (b) schematic of the two-channel OSS designed for the proof of principle demonstration of simultaneously generating two chirped microwave waveforms with different characteristics.

B. Multi-channel OSS based on an AWGSI

The second OSS design is based on an AWGSI incorporating LCWBGs and the general schematic for multi-channel operation is shown in Fig. 4(a). For a proof of principle demonstration, we consider a two-channel OSS incorporating LCWBG₁ and LCWBG₂ in the two separate branches of the AWGSI for simultaneous generation of two chirped microwave waveforms, see Fig. 4(b). After splitting the input power into two paths via a 3-dB multimode interference (MMI) coupler, each path enters to one branch of the AWGSI, is reflected back from the LCWBGs, and then recombined in the MMI coupler. Each branch of the AWGSI generates one independent chirped microwave waveform with the profile defined by the patch imbalance and the grating chirp of the involved LCWBG.

LCWBG₁ has a path imbalance of $\Delta L_1 = L_{11} - L_{12}$ in the Sagnac loop where L_{11} and L_{12} are the two path lengths from LCWBG₁ to the MMI coupler. Similarly LCWBG₂ has a path imbalance of $\Delta L_2 = L_{21} - L_{22}$. If the LCWBG is at the center of the Sagnac loop, $\Delta L_i = 0$ ($i = 1, 2$).

The central frequency and the RF chirp of each generated chirped microwave waveform can be calculated from (3) considering the effective cavity length of the Sagnac loop. The effective cavity length consists of the wavelength-independent path imbalance (ΔL_i) and the wavelength-dependent grating length difference (ΔL_λ) where $\Delta L_\lambda = (\lambda - \lambda_c)/C$ where λ_c is the center wavelength and C is the grating chirp [22, 23]. The effective cavity length of the Sagnac loop can be obtained as:

$$\Delta L_{eff} = \Delta L + \frac{\lambda - \lambda_c}{C} \quad (6)$$

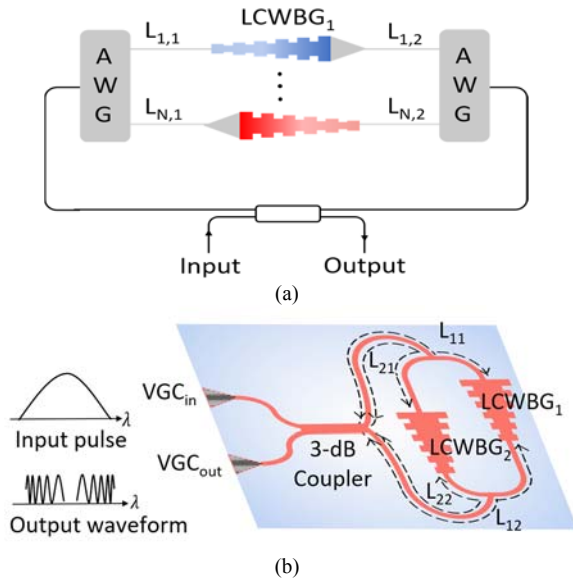


Fig. 4. (a) General schematic of integrated multi-channel OSS based on an AWGSI incorporating multiple LCWBGs and (b) schematic of the two-channel OSS designed for the proof of principle demonstration of simultaneously generating two chirped microwave waveforms with different characteristics.

To generate two chirped microwave waveforms at the same central frequency with opposite signs of RF chirp, we considered two LCWBGs having the same grating chirp and with the same magnitude of path imbalance, but placed in opposite locations relative to the center of the Sagnac loop, i.e., $\Delta L_1 \Delta L_2 < 0$. We designed two OSSs; one of them (OSS-3) uses $\Delta L_1 = -\Delta L_2 = 2$ mm and incorporates LCWBG-A₁ to generate a waveform at shorter wavelengths with a positive RF chirp, and LCWBG-A₂ to generate a waveform at longer wavelengths with a negative RF chirp. The second OSS (OSS-4) uses $\Delta L_1 = -\Delta L_2 = -2$ mm and incorporates LCWBG-B₁ to generate a waveform at shorter wavelengths with a negative RF chirp, and LCWBG-B₂ to generate a waveform at longer wavelengths with a positive RF chirp.

Tables II and III summarize the parameters of all four OSSs.

TABLE II
PARAMETERS OF THE OSSS BASED ON THE DFPCs

		LCWBG	L_{offset} [nm]	L_c [nm]	W_c [nm]
OSS-1	DFPC ₁	A ₁	591	300	740
	DFPC ₂	A ₂	894	600	720
OSS-2	DFPC ₁	B ₁	614	600	520
	DFPC ₂	B ₂	918	300	510

TABLE III
PARAMETERS OF THE OSSS BASED ON THE AWGSI

		LCWBG	ΔL [mm]
OSS-3	LCWBG ₁	A ₁	+2
	LCWBG ₂	A ₂	-2
OSS-4	LCWBG ₁	B ₁	-2
	LCWBG ₂	B ₂	+2

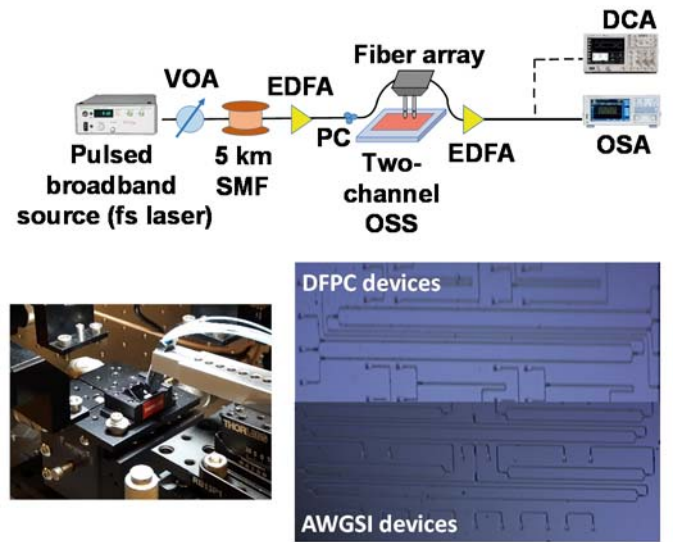


Fig. 5. Schematic and photo of experimental setup for generating multi-channel WDM chirped microwave waveforms. CCD camera images of the chip showing different DFPC (top) and AWGSI (bottom) devices.

III. EXPERIMENTAL SETUP AND RESULTS

The schematic of our experimental setup is shown in Fig. 5. A broadband pulse generated by a 20 MHz femtosecond mode-locked laser passes through a 5 km spool of single mode fiber (SMF) having a dispersion of 85 ps/(nm·km) at 1550 nm for WTM. The broadband pulse is amplified to 8 dBm and coupled to the integrated OSSs by means of a fiber ribbon array. The angle of the fiber ribbon array is adjusted so that the response of the VGCs are centered with the spectral responses of the OSSs. The fiber-to-fiber insertion loss of the OSS is ~25 dB while the OSS itself introduces ~10 dB loss. A polarization controller (PC) is used to optimize the response and EDFAs are used to compensate losses. The spectral response is recorded by an optical spectrum analyzer (OSA) with a resolution of 50 pm. The temporal response of the waveform is detected by a 65 GHz bandwidth optical sampling module connected to a digital communications analyzer (DCA) in sample mode operation with a persistence time of 300 ms. After the waveforms are

recorded, they are processed offline using MATLAB to calculate the spectrogram (time-frequency) representations and compressed pulse (correlation). The spectrogram representations are obtained using the function *pspectrum* and the parameters are adjusted to provide a compromise in resolution between the time and frequency domains.

Figures 6 and 7 summarize the experimental results of the four multi-channel OSSs.

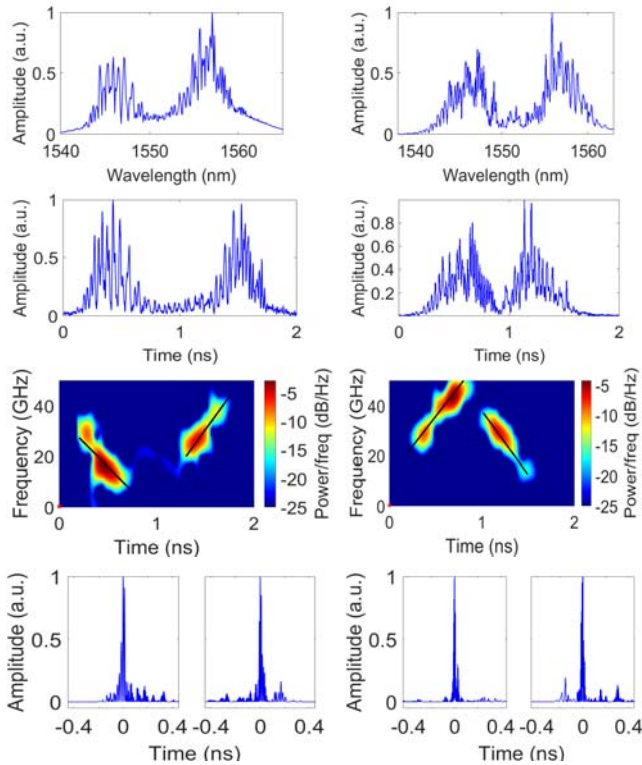


Fig. 6. (a) Spectrum, (b) temporal, (c) spectrogram, and (d) correlation results of OSS-1 (left) and OSS-2 (right).

The measured spectral and temporal responses, as well as calculated spectrograms and correlations (compressed pulses) for the waveforms generated using the parallel DFPCs, i.e., OSS-1 and OSS-2, are shown in Fig. 6. The spectrograms corresponding to the two temporal waveforms indicate that two independent chirped microwave waveforms with different central frequencies and opposite signs of RF chirp are generated. For OSS-1, the two waveforms have central frequencies of 21 GHz and 31 GHz and corresponding RF chirps of -52 GHz/ns and +49 GHz/ns. For OSS-2, the two waveforms have central frequencies of 36 GHz and 24 GHz and corresponding RF chirps of +46 GHz/ns and -51 GHz/ns.

The measured spectral and temporal responses and calculated spectrograms and correlations for the waveforms generated using OSS-3 and OSS-4 appear in Fig. 7. The spectrograms show the generation of the two chirped microwave waveforms with the same central frequency due to the same amount of the path imbalance, yet opposite signs of RF chirp due to the location of the path imbalances in opposite directions relative to the center of the Sagnac loop. OSS-3

generates two waveforms with the central frequencies of 70 GHz and 67 GHz with the RF chirps of +27 GHz/ns and -29 GHz/ns. OSS-4 generates two waveforms with the central frequencies of 69 GHz and 66 GHz with the RF chirps of -25 GHz/ns and +25 GHz/ns. Note that the central frequencies are different from those of the waveforms generated using OSS-1 and OSS-2 since the values of L_{offset} are different. The large variation in amplitudes between the two waveforms can come from the spectral response of the EDFA as well as the VGCs (which vary when we optimize the coupling angle). Additional adjustment of the experimental setup and parameters will reduce these variations; it is also possible to compensate for the difference using a programmable filter after the output EDFA (e.g., Finisar Waveshaper) or after demultiplexing the waveforms.

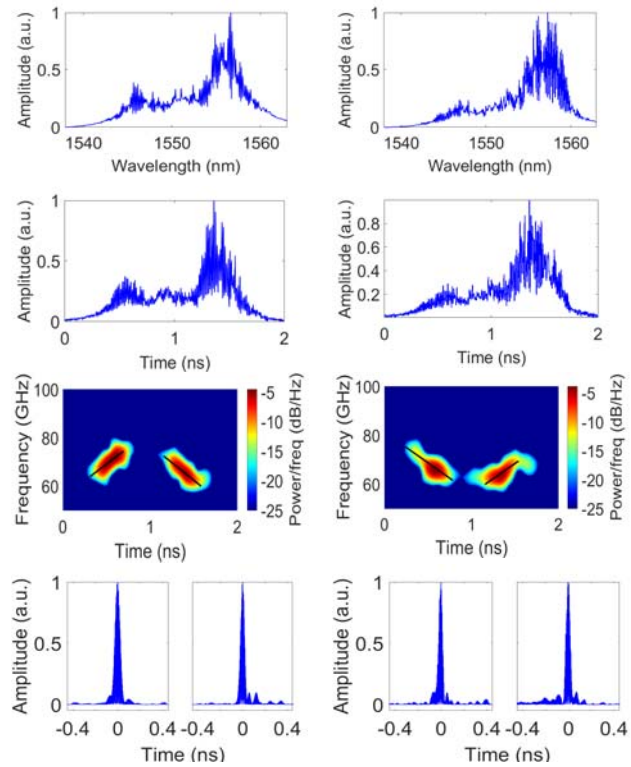


Fig. 5. (a) Spectrum, (b) temporal, (c) spectrogram, and (d) correlation results of OSS-3 (left) and OSS-4 (right).

Note that the spectra show rather strong ripples. These ripples are due to the spectral response of the individual LCWBGs in the OSSs (which, in turn, arise from errors in fabrication such as roughness on the sidewall corrugations from etching) as well as reflections from the VGCs and other parts of the device which can create FP resonances. The ripples, which translate into ripples in the temporal waveforms, can contribute to greater sidelobes in the compressed pulses (the impact of the ripples in the spectral will be 'smoothed out' due to WTM and the bandwidth of the photodetector used to record the temporal waveforms). The ripples can be reduced through improved fabrication.

Generally, the TBWP of the chirped microwave waveforms can be estimated by $\left(\frac{4n_{eff}}{\lambda_0}\right) Cl^2$ where l is the length of the

LCWBG [21]. The TBWPs of the generated waveforms for OSS-1 are ~ 6 and 5.7 and those for OSS-2 are ~ 6.7 and 7.5. The estimated TBWPs of the generated waveforms for OSS-3 are ~3.1 and 3.4 and for OSS-4 are both ~3.7. The TBWPs are quite small due to the very short grating lengths used (~ 0.3 mm). To improve the TBWP, we need to optimize the grating chirp and length further. For example, Zhang and Yao obtained a TBWP in excess of 600 using LCWBGs with a grating chirp of ~1.6 nm/mm and a length of 12.54 mm [15, 16]. While our LCWBGs have a grating chirp that is ~9 times larger (~14 nm/mm compared to ~1.6 nm/mm), they are ~42 times shorter (~0.3 mm compared to 12.54 mm). The TBWPs obtained in [15, 16] are nearly 200 times greater than those that we obtained, which is in agreement with the fact that the TBWP scales with Cl^2 . We also note that reducing imperfections from fabrication and improving LCWBG design, e.g., using rib waveguides rather than strip waveguides (as in [15, 16]) can improve the linearity of the generated waveforms.

Tables IV and V summarize the calculated and measured values for the chirp rate and central frequency of the waveforms generated by the OSSs. The results are generally in agreement with each other and the differences arise due to fabrication errors, uncertainty in grating chirp, and uncertainty in estimating the actual path imbalance.

IV. DISCUSSION

We have demonstrated two multi-channel integrated OSSs based on parallel DFPCs and an AWGSI incorporating LCWBGs. The following are the key features of our devices:

1. They can be used to generate simultaneously two WDM chirped microwave waveforms that have different characteristics;
2. The central frequencies and RF chirps of the generated waveforms can be set easily through the device parameters, e.g., grating chirp, cavity length, or path imbalance;
3. Since the waveforms are wavelength multiplexed, they can be separated easily using optical filters which may provide increased functionality, e.g., switching between range or resolution, in imaging applications; and
4. The structures are simple and based on LCWBGs which are compact.

In contrast, there are several disadvantages such as the following:

1. The total bandwidth that is available for spectral shaping is constrained by the bandwidth of the VGCs used for input and output coupling;
2. Increasing the number of channels will ultimately be limited by the bandwidth of the VGCs and/or the optical bandwidth that results from optimal grating design to achieve high TBWP; and
3. The central frequencies and RF chirp are fixed by the device parameters.

It is possible to tune the spectral response of the OSSs so that the central frequency and/or RF chirp (magnitude and sign) of the generated waveforms can be varied. We can tune the LCWBGs using thermal or electro-optic effects in both OSS designs, [15, 16, 24]. Moreover, in the OSS design based on an AWGSI, it is possible to apply metal heaters on both sides of an LCWBG that is located at the center of the loop. Independent

control over these two heaters will allow for precise tuning of the amount of path imbalance as well as the sign which, in turn, will allow for changing the central frequency and sign of the RF chirp of the generated waveform. As an example, if we heat the 2 mm long waveguide segments used to create the path imbalances in the AWGSI and consider a temperature change of 30 °C, this creates a change in optical path length of 0.012 mm and correspondingly, a change in central frequency of 310 MHz. Greater changes are possible by heating longer path imbalances. On the other hand, the OSS based on the DFPC will have limited capability to tune the central frequency of the generated waveform due to the relatively short (physical) cavity length of the DFPC (which will constrain the ability to vary this optical cavity length). Moreover, by using electro-optic effects with pn junction waveguides, it will be possible to tune the chirp of the LCWBG and hence, the amount of RF chirp (assuming that a fixed amount of dispersion is used for WTM). For example, using a 7 mm long chirped grating in a rib waveguide with a lateral pn junction, Zhang and Yao demonstrated tuning of the grating dispersion by up to 1.4 ps/nm for an applied voltage of 20 V [16]. This allowed the RF chirp of the generated chirped microwave waveforms to be tuned by a fraction of 1 GHz/ns. The reconfiguration speed of the OSS will depend on whether thermal or electro-optic effects are utilized; the latter support higher speeds of operation.

TABLE IV

MEASURED (CALCULATED) CHIRP RATE ($\frac{df_{RF}(t)}{dt}$), CENTRAL FREQUENCY (f_c)

	First waveform (on the left)		Second waveform (on the right)	
	$\left \frac{df_{RF}(t)}{dt}\right $ (GHz/ns)	f_c (GHz)	$\left \frac{df_{RF}(t)}{dt}\right $ (GHz/ns)	f_c (GHz)
OSS-1	-52 (-45)	21 (23)	+49 (+45)	31 (31)
OSS-2	+46 (+40)	36 (30)	-51 (-40)	24 (22)

TABLE V

MEASURED (CALCULATED) CHIRP RATE ($\frac{df_{RF}(t)}{dt}$), CENTRAL FREQUENCY (f_c)

	First waveform (on the left)		Second waveform (on the right)	
	$\left \frac{df_{RF}(t)}{dt}\right $ (GHz/ns)	f_c (GHz)	$\left \frac{df_{RF}(t)}{dt}\right $ (GHz/ns)	f_c (GHz)
OSS-3	+27 (+22)	70 (52)	-29 (-22)	67 (51)
OSS-4	-25 (-20)	69 (48)	+25 (+20)	66 (48)

V. SUMMARY

We have demonstrated the simultaneous generation of WDM chirped microwave waveforms with different characteristics using integrated multi-channel OSSs and WTM. We designed and tested two different OSSs, one based on parallel DFPCs and one based on an AWGSI incorporating LCWBGs. The OSSs based on DFPCs generated two chirped microwave waveforms with different central frequencies and opposite RF chirps while the OSSs based on an AWGSI generated two chirped microwave waveforms at the same central frequency and opposite signs of RF chirp. Our work is significant as it highlights the feasibility for simultaneous generation of WDM chirped microwave waveforms which may provide the advantages offered by multiple channels, e.g., increasing functionality or capability of systems; moreover, integrated

brings the advantages of stability, compactness, and potential for tuning.

REFERENCES

- [1] H. Peng and D. C. Liu, "Enhanced ultrasound strain imaging using chirped pulse excitation," *Biomedical Signal Processing and Control*, vol. 8, no. 2, p. 130-141, Mar. 2013
- [2] J. W. Shi, F. M. Kuo, N. W. Chen, S. Y. Set, C. B. Huang, J. E. Bowers, "Photonic generation and wireless transmission of linearly/nonlinearly continuously tunable chirped millimeter-wave waveforms with high time-bandwidth product at w-band," *IEEE Photonics Journal*, vol. 4, no. 1, pp. 215-223, Feb. 2012.
- [3] A. Rashidinejad and A. M. Weiner, "Photonic radio-frequency arbitrary waveform generation with maximal time-bandwidth product capability," *IEEE/OSA Journal of Lightwave Technology*, vol. 32, no. 20, pp. 3383-3393, Oct. 2014.
- [4] P. Dong, Y. K. Chen, G. H. Duan, and D. T. Neilson, "Silicon photonic devices and integrated circuits," *Nanophotonics*, vol. 3, no. 45, pp. 215-228, Aug. 2014.
- [5] J.-M. Wun, C.-C. Wei, J. Chen, C. S. Goh, S. Y. Set, and J.-W. Shi, "Photonic chirped radio-frequency generator with ultra-fast sweeping rate and ultra-wide sweeping range," *Optics Express*, vol. 21, no. 9, pp. 11475-11481, May 2013.
- [6] F. Zhang, Q. Guo, Y. Zhang, Y. Yao, P. Zhou, D. Zhu, and S. Pan, "Photonics-based real-time and high-resolution ISAR imaging of non-cooperative target," *Chinese Optics Letters*, vol. 15, no. 11, pp. 112801, Nov. 2017.
- [7] J. D. McKinney, D. Seo, D. E. Leaird, and A. M. Weiner, "Photonically assisted generation of arbitrary millimeter-wave and microwave electromagnetic waveforms via direct space-to-time optical pulse shaping," *IEEE/OSA Journal of Lightwave Technology*, vol. 21, no. 12, pp. 3020-3028, Dec. 2003.
- [8] C. Wang, M. Li, and J. Yao, "Continuously tunable photonic microwave frequency multiplication by use of an unbalanced temporal pulse shaping system," *IEEE Photonics Technology Letters*, vol. 22, no. 17, pp. 1285-1287, Sep. 2010.
- [9] J. Yao, "Photonic generation of microwave arbitrary waveforms," *Optics Communications*, vol. 284, no. 15, pp. 3723-3736, Jul. 2011.
- [10] A. Rashidinejad, Y. Li, and A. M. Weiner, "Recent advances in programmable photonic-assisted ultrabroadband radio-frequency arbitrary waveform generation," *IEEE Journal of Quantum Electronics*, vol. 52, no. 1, pp. 1-17, Jan. 2016.
- [11] T. K. Song and Y. K. Jeong, "Ultrasound imaging system and method based on simultaneous multiple transmit-focusing using weighted orthogonal chirp signals," US Patent 7,066,886, Jun. 27 2006.
- [12] P. Moslemi and L. R. Chen, "Simultaneously generating multiple chirped microwave pulses with superimposed FBGs," *IEEE Photonics Technology Letters*, vol. 29, no. 16, pp. 1387-1390, Aug. 2017.
- [13] P. Moslemi, L. R. Chen, and M. Rochette, "Simultaneously generating multiple chirped microwave waveforms using an arrayed waveguide Sagnac interferometer," *Electronics Letters*, vol. 53, no. 23, pp. 1534-1535, Nov. 2017.
- [14] W. Zhang, J. Zhang, and J. Yao, "Largely chirped microwave waveform generation using a silicon-based on-chip optical spectral shaper," in Microwave Photonics (MWP) and the 2014 9th Asia-Pacific Microwave Photonics Conference (APMP), *IEEE International Topical Meeting on*, pp. 51-53, Oct. 2014.
- [15] W. Zhang and J. Yao, "Silicon-based on-chip electrically-tunable spectral shaper for continuously tunable linearly chirped microwave waveform generation," *Journal of Lightwave Technology*, vol. 34, no. 20, pp. 4664-4672, Oct. 2016.
- [16] W. Zhang and J. P. Yao, "Photonic generation of linearly chirped microwave waveforms using a silicon-based on-chip spectral shaper incorporating two linearly chirped waveguide Bragg gratings," *IEEE/OSA J. Lightw. Technol.*, vol. 33, no. 24, pp. 5047-5054, Dec. 2015.
- [17] J. Wang, H. Shen, L. Fan, R. Wu, B. Niu, L. T. Varghese, Y. Xuan, D. E. Leaird, X. Wang, F. Gan, A. M. Weiner, "Reconfigurable radio-frequency arbitrary waveforms synthesized in a silicon photonic chip," *Nature communications*, vol. 6, Jan. 2015.
- [18] M. Ma, M. Rochette, and L. R. Chen, "Generating chirped microwave pulses using an integrated distributed Fabry-Pérot cavity in silicon-on-insulator," *IEEE Photonics Journal*, vol. 7, no. 2, pp. 1-6, Apr. 2015.
- [19] J. Wang, R. Ashrafi, M. Rochette, and L. R. Chen, "Chirped microwave pulse generation using an integrated SiP Bragg grating in a Sagnac loop," *IEEE Photonics Technology Letters*, vol. 27, no. 17, pp. 1876-1879, Sep. 2015.
- [20] Y. Wang, X. Wang, J. Flueckiger, H. Yun, W. Shi, R. Bojko, N. A. F. Jaeger, and L. Chrostowski, "Focusing sub-wavelength grating couplers with low back reflections for rapid prototyping of silicon photonic circuits," *Optics express*, vol. 22, no. 17, pp. 20652-20662, Aug. 2014.
- [21] C. Wang, J. Yao, "Photonic generation of chirped microwave pulses using superimposed chirped fiber Bragg gratings," *IEEE Photonics Technology Letters*, vol. 20, no. 11, p. 882-884, Jun. 2008.
- [22] L. R. Chen, "Photonic generation of chirped microwave and millimeter wave pulses based on optical spectral shaping and wavelength-to-time mapping in silicon photonics," *Optics Communications*, vol. 373, pp. 70-81, Aug. 2016.
- [23] C. Wang and J. Yao, "Chirped microwave pulse generation based on optical spectral shaping and wavelength-to-time mapping using a Sagnac loop mirror incorporating a chirped fiber Bragg grating," *IEEE/OSA Journal of Lightwave Technology*, vol. 27, no. 16, pp. 3336-3341, Aug. 2009.
- [24] W. Zhang, N. Ehteshami, W. Liu, and J. Yao, "Silicon-based on-chip electrically tunable sidewall Bragg grating Fabry-Pérot filter," *Optics Letters*, vol. 40, no. 13, pp. 3153-3156, Jul. 2015.

Parisa Moslemi (M'16) received the B.Eng. degree in electrical and computer engineering from Isfahan University of Technology, Isfahan, Iran in 2009 and the M.A.Sc. degree in 2012 from École de technologie supérieure (Université du Québec), Montreal, QC, Canada. In 2014, she started her Ph.D. degree at McGill University, Montreal, QC, Canada. Her research interests are in microwave photonics, optical communications, fiber and integrated optics, and microwaves and antennas.

Martin Rochette (M'07, SM'13) received the B.A.Sc. degree in physics engineering at Laval University (Ste. Foy, QC, Canada) in 1995. Then with the Department of Electrical and Computer Engineering of Laval University, he made collaborative M.Eng. and Ph.D. degrees with Exfo engineering in 1995-1997 and the National Optics Institute in 1997-2001, respectively. From 2001 to 2003, he was working in the optical communication industry as a technology leader in the design and performance optimization of optical components and access systems. From 2003 to 2006, he was a fellow researcher successively in telecommunications at the department of Electrical and Computer Engineering at Laval University and in the applications of nonlinear optics in the Departments of physics at the University of Sydney in Australia. Since 2006, he has been with the Department of Electrical and Computer Engineering at McGill University in Montreal, QC, Canada. He published over 200 journal and conference papers about highly nonlinear materials and devices, fiber laser sources, optical fiber components and optical communication systems. His current research interests include the application of nonlinear effects for devices and laser sources with applications for biomedicine, instrumentation and telecommunication systems.

Lawrence R. Chen (S'95, SM'05) received the B.Eng. degree in electrical engineering and mathematics from McGill University, Montreal, QC, Canada in 1995 and the M.A.Sc. and Ph.D. degrees in electrical and computer engineering from the

University of Toronto, Toronto, ON, Canada in 1997 and 2000, respectively. Since 2000, he has been with the Department of Electrical and Computer Engineering at McGill University. His research interests are in optical communications, fiber and integrated optics, and microwave photonics (in particular, active and passive devices in silicon photonics for optical and microwave signal processing) as well as engineering education and teaching pedagogy.

Dr. Chen is the former Editor-in-Chief for the *IEEE Photonics Newsletter*, a former Topical Editor of *Optics Letters*, an Editor of *Optics Communications*, and a Subject Editor of *IET Electronics Letters*. He is a Fellow of the Optical Society of America.